

Long-term evolution of BH-ULX candidates: an ‘unusual’ $L_{\text{disc}}-T_{\text{col}}$ correlation associated with spectral states

Seshadri Majumder¹*, Santabrata Das¹ and Anuj Nandi²

¹Department of Physics, Indian Institute of Technology Guwahati, Guwahati 781039, India

²Space Astronomy Group, ISITE Campus, U. R. Rao Satellite Centre, Outer Ring Road, Marathahalli, Bangalore 560037, India

Accepted 2025 April 11. Received 2025 April 9; in original form 2024 December 11

ABSTRACT

We present the long-term spectral evolution of eight black hole ultraluminous X-ray sources (BH-ULXs), namely NGC 1313 X-1, NGC 5408 X-1, NGC 6946 X-1, IC 342 X-1, NGC 55 ULX-1, NGC 4395 ULX-1, NGC 5204 X-1, and NGC 4190 ULX-1 using *XMM-Newton* monitoring data spanning over a decade or more. An in-depth spectral modelling with thermal Comptonization (nthComp) and standard disc (diskbb) components reveals NGC 5204 X-1, IC 342 X-1, NGC 4190 ULX-1, and NGC 1313 X-1 exhibiting harder spectral characteristics with dominant effect of Comptonization ($F_{\text{nth}} > F_{\text{disc}}$, $\Gamma_{\text{nth}} \lesssim 2$). However, NGC 6946 X-1 and NGC 55 ULX-1 remain in a disc-dominated state ($F_{\text{disc}} \sim 2F_{\text{nth}}$, $\Gamma_{\text{nth}} \gtrsim 2$), while NGC 5408 X-1 shows intermediate spectral characteristics. The spectral analyses indicate an anticorrelation between disc luminosity (L_{disc}) and temperature (T_{col}) for all sources except NGC 5204 X-1. These anticorrelations follow a relation $L_{\text{disc}} \propto T_{\text{col}}^{\alpha}$ with steeper exponents of $\alpha = -6.01 \pm 0.25$ (NGC 55 ULX-1), $\alpha = -8.93 \pm 0.11$ (NGC 6946 X-1), and $\alpha = -10.31 \pm 0.10$ (NGC 5408 X-1) for sources with softer or intermediate spectral characteristics. For harder sources, NGC 1313 X-1 and IC 342 X-1, the combined results provide $\alpha = -3.58 \pm 0.04$. However, for NGC 5204 X-1, a positive correlation is found, yielding $\alpha = 1.4 \pm 0.1$, suggesting that the emission mechanism is associated with the transition from the ‘standard disc’ to the ‘slim disc’ scenario. These findings suggest that the observed $L_{\text{disc}}-T_{\text{col}}$ correlations, along with the overall spectrottemporal properties of BH-ULXs, seem to be governed by disc–corona–wind-driven accretion processes at various inclinations. Finally, we report a quasi-periodic oscillation like feature (~ 20 mHz) with rms percentage ~ 6.6 , Q -factor ~ 6.7 , and significant 2.8σ in NGC 55 ULX-1.

Key words: accretion, accretion discs – black hole physics – radiation mechanisms: general – stars: individual: NGC 1313 X-1 – stars: individual: NGC 5408 X-1 – X-rays: galaxies.

1 INTRODUCTION

Ultraluminous X-ray sources (ULXs) are a class of extragalactic, point-like, non-nuclear objects with isotropic luminosity in excess of 10^{39} erg s^{−1} (Fabbiano 1989; Makishima et al. 2000). Despite being discovered more than 30 yr ago, the exact nature of these objects remains a point of debate, and their observational features are still not well understood (see Feng & Soria 2011; Kaaret, Feng & Roberts 2017; Fabrika et al. 2021; King, Lasota & Middleton 2023, for a recent review). Based on the observational evidence from timing and spectral variability, a population of ULXs is believed to be powered by super-Eddington accretion onto stellar-mass black holes (Bachetti et al. 2013; Walton et al. 2013, 2014, 2015; Rana et al. 2015, see references therein). The presence of massive stellar-mass black holes in several ULXs is also suggested (Agrawal & Nandi 2015; Das et al. 2021; Majumder et al. 2023). Alternatively, a plausible scenario relying on the intermediate-mass black holes (IMBHs) of mass $\gtrsim 100 M_{\odot}$ as the powerhouse of such extremely luminous systems is also propounded (Colbert & Mushotzky 1999;

Makishima et al. 2000; Miller et al. 2003; Das et al. 2021; Majumder et al. 2023). In addition, the possibility of having highly magnetized neutron stars at the central core is also put forward to explain the pulsations detected in several ULXs (Bachetti et al. 2014; Fürst et al. 2016; Israel et al. 2017; Carpano et al. 2018; Sathyaprakash et al. 2019; Rodríguez Castillo et al. 2020; Quintin et al. 2021).

The temporal variability of ULXs has been studied in several sources over the past few decades. However, the interpretation of the physical origin of these variability properties remains challenging. For example, based on the observed variability in the power density spectra, Heil, Vaughan & Roberts (2009) proposed that a sample of bright ULXs of comparable luminosity can be divided into two groups – one showing very weak variability on the time-scale of about 100 s, whereas another exhibiting similar variability properties, observed in most of the black hole X-ray binaries (BH-XRBs; Belloni et al. 2005; Nandi et al. 2012; Athulya et al. 2022; Aneesha et al. 2024). Intriguingly, the mechanism that suppresses the intrinsic variability in one group of ULXs remains under debate (Heil et al. 2009; Feng & Soria 2011). Interestingly, the fractional variability amplitude (f_{var}), indicative of the amount of variability, is found to be low ($\lesssim 10$ per cent) in the hard-ultraluminous (HUL) states as compared to the soft-ultraluminous (SUL) states with $f_{\text{var}} \sim$

* E-mail: smajumder@iitg.ac.in

10–30 per cent (Sutton, Roberts & Middleton 2013). Further, several ULXs are also reported to exhibit quasi-periodic oscillations (QPOs) in the presence of flat-topped noise in the power density spectra (Dewan, Titarchuk & Griffiths 2006; Strohmayer et al. 2007; Feng, Rao & Kaaret 2010; Rao, Feng & Kaaret 2010; Agrawal & Nandi 2015; Pasham et al. 2015; Atapin, Fabrika & Caballero-García 2019; Majumder et al. 2023). In addition, it has been proposed that the observed QPOs are possibly generated due to the modulation of the Comptonizing corona, present at the inner accretion flow, and that serves as a powerful tool to probe the accretion scenarios of the ULXs harbouring black hole accretors (Das et al. 2021; Majumder et al. 2023).

Needless to mention that the spectral morphologies of ULXs are well studied in X-rays with dedicated missions like *XMM-Newton*, *Chandra*, and *NuSTAR* over the years. Interestingly, the ULX spectra up to ~ 10 keV can be classified into two distinct types: one described by a simple power law and the other exhibiting a broad spectral curvature over the entire energy band (Feng & Soria 2011). Generally, a high power-law photon index of $\Gamma \gtrsim 3$ is seen for the sources of softer characteristics, whereas $\Gamma \sim 1$ is observed in a few harder sources. Notably, some of the hard power-law-dominated ULXs show significant flux variability (Feng & Kaaret 2009; Kaaret & Feng 2009; Soria & Ghosh 2009) similar to the hard state of BH-XRBs (Belloni et al. 2005; Remillard & McClintock 2006). Thus, the interpretation of power-law-dominated spectral state in ULXs as the canonical hard state of BH-XRBs would imply a black hole of mass $\gtrsim 10^3 M_\odot$ (Winter, Mushotzky & Reynolds 2006; Feng & Soria 2011). Meanwhile, a good number of high-quality observations from *XMM-Newton* could detect the soft excess in low energies (< 2 keV) and curvature around ~ 3 – 10 keV in ULX spectra (Ghosh & Rana 2021, and references therein) unlike the BH-XRBs, showing a spectral turnover at relatively higher energies (Xu et al. 2019). Further, it has been suggested that the high-energy curvature could arise from the innermost hot accretion flow as a result of the interception of disc photons into the Comptonizing corona (Middleton et al. 2015; Mukherjee et al. 2015; Jithesh 2022). In contrast, the soft excess below ~ 2 keV is thought to originate from the outflowing wind or entirely from the disc emission alone (Poutanen et al. 2007; Middleton et al. 2015).

The extensive monitoring with *XMM-Newton*, *Chandra*, *NuSTAR*, and *Swift*-X-Ray Telescope (XRT) enables the opportunity of studying the long-term spectrottemporal evolution of ULXs. So far, a handful of sources have been studied in quest of the long-term variation of ULX characteristics. For example, Gúrpide et al. (2021) reported the spectral evolution for a group of ULXs, revealing the origin of variability in these systems. In addition, the transition between several spectral states is conjectured from the long-term monitoring of a number of ULXs (Yoshida et al. 2010). Further, the long-term monitoring of NGC 5408 X-1 with *Swift*-XRT reveals dipping behaviour in the light curve, possibly connected to the superorbital phenomenon, similar to some of the BH-XRBs (Grisé et al. 2013).

In this work, we consider eight BH-ULXs, namely NGC 1313 X-1, NGC 5408 X-1, NGC 6946 X-1, IC 342 X-1, NGC 55 ULX-1, NGC 4395 ULX-1, NGC 5204 X-1, and NGC 4190 ULX-1, having decade-long observations with *XMM-Newton*. The sources are primarily selected based on the publicly available *XMM-Newton* observations spanning over about a decade and the previous predictions of having black hole accretors at the central core of these objects. Out of these eight sources, a detailed spectrottemporal study is carried out for five sources (NGC 1313 X-1, NGC 5408 X-1, NGC 6946 X-1, M82 X-1, and IC 342 X-1) that show mHz QPO features (Majumder et al.

2023, hereafter Paper I). Note that the BH-ULX candidate NGC 247 ULX-1 was not studied in Paper I due to the absence of any reported QPO detections for this source. It is worth mentioning that M82 X-1 is kept aside from this work irrespective of having multiple observations because of the significant contamination from nearby objects in the *XMM-Newton* aperture (see Paper I and references therein). Moreover, a preliminary analysis of the variability properties of NGC 247 ULX-1 suggests that the source exhibits a dipping behaviour in its light curves (see also Alston et al. 2021), accompanied by supersoft characteristics, which remain distinct from those of other sources. Therefore, we exclude NGC 247 ULX-1 in this study. Note that the four sources, namely NGC 55 ULX-1, NGC 4395 ULX-1, NGC 5204 X-1, and NGC 4190 ULX-1, have been relatively less studied and serve as ideal targets for detailed analysis. With the exception of the above source selection criteria, NGC 4190 ULX-1 – often referred to as the ‘forgotten ULX’ due to its intriguing yet relatively unexplored characteristics – is also considered in this work, despite having only three observations with *XMM-Newton*. Below, we present the brief characteristics of the four sources for which an in-depth analysis has been performed in this work.

(i) NGC 55 ULX-1 is the brightest ULX in the spiral galaxy NGC 55 at a distance of 1.94 Mpc¹ with a peak luminosity of $\sim 4 \times 10^{39}$ erg s⁻¹. Interestingly, in most of the previous studies, the source was found in the SUL state with disc-dominated spectra (Barra et al. 2022; Jithesh 2022).

(ii) NGC 4395 ULX-1 is one of the ULXs located in the NGC 4395 galaxy at a distance of 4.76 Mpc with luminosity $\sim 3 \times 10^{39}$ erg s⁻¹ (Ghosh, Rana & Bachetti 2022). Detailed spectral study with *XMM-Newton* and *Chandra* observations rules out the possibility of having an SUL state by confirming its steep power-law tail (Earnshaw & Roberts 2017).

(iii) The source NGC 5204 X-1 is located ~ 15 arcsec away from the centre of the host galaxy NGC 5204 at a distance of 4.8 Mpc. The evidence of significant outflows resulting in several emission features is observed in NGC 5204 X-1 with *XMM-Newton* (Kosec et al. 2018).

(iv) The low surface brightness galaxy NGC 4190 located at a distance of 3 Mpc contains NGC 4190 ULX-1, a bright ULX of luminosity $\sim (3\text{--}10) \times 10^{39}$ erg s⁻¹ (Ghosh & Rana 2021). The mass of the source is predicted to be in the range of 10–30 M_\odot , indicating the presence of a stellar-mass black hole in the system (Ghosh & Rana 2021). Recently, a super-Eddington slim disc scenario is also been suggested for NGC 4190 ULX-1 (Earnshaw et al. 2024).

In this work, we carry out a detailed long-term spectrottemporal analysis of the selected BH-ULXs using the archival *XMM-Newton* observations spanning over a decade. Towards this, we investigate the spectral characteristics of the sources by modelling the *XMM-Newton* spectra in 0.3–10 keV energy range with the combination of physically motivated models, describing different emission mechanisms. Investigation of the spectral properties indicates the presence of both positive and negative correlations between the bolometric disc luminosity (L_{disc}) and the disc temperature. The correlation properties are observed to be closely connected with the distinct spectral states, obtained from the long-term evolution of the sources. Finally, we find that the disc–corona–wind-regulated accretion scenario described by the Keplerian and sub-Keplerian flow components is capable of explaining the spectrottemporal findings of the BH-ULXs.

¹<https://ned.ipac.caltech.edu>

The paper is organized as follows. In Section 2, we briefly mention the *XMM-Newton* observations of the sources and the standard data reduction procedure of the European Photon Imaging Camera-pn (EPIC-pn) and EPIC-MOS instruments. The results of spectral and timing analyses are presented in Section 3. In Section 4, we infer the possible physical scenarios to delineate the findings and summarize the results in Section 5.

2 OBSERVATION AND DATA REDUCTION

We look into the HEASARC public data archive² for all the observations of NGC 55 ULX-1, NGC 4395 ULX-1, NGC 5204 X-1, and NGC 4190 ULX-1 with *XMM-Newton*. We find that the sources are observed on several occasions by *XMM-Newton* and, except NGC 4190 ULX-1, all the sources have at least 10 or 20 yr of monitoring. In Table 1, we tabulate the details of all the observations considered in this work. We find a total of 31 observations considering all the sources. However, we note that several observations suffer from various caveats (see ‘Remarks’ column in Table 1) and hence are excluded from the analysis.

The *XMM-Newton* data extraction of the remaining observations is carried out following the analysis threads³ provided by the instrument team. The data reduction software Science Analysis System (SAS) v21.0.0⁴ is used to analyse the data. We run the tasks `epproc` and `emproc` to generate the event files for EPIC-pn and EPIC-MOS instruments, respectively. The high-energy particle background flares are identified and clean event files are filtered out following Paper I. We adopt the event selection criteria as `PATTERN` ≤ 4 and `PATTERN` ≤ 12 with `FLAG` = 0 while generating the scientific products from EPIC-pn and EPIC-MOS data, respectively. Following the previous studies, we select the source regions while extracting the light curves and spectra as 40, 25, 30, and 40 arcsec for NGC 55 ULX-1 (Jithesh 2022), NGC 4395 ULX-1 (Ghosh et al. 2022), NGC 4190 ULX-1 (Ghosh & Rana 2021), and NGC 5204 X-1 (Gúrpide et al. 2021), respectively. Further, we select the same circular radii for the respective sources in a source-free area on the same EPIC chip to generate the background light curves and spectra. For spectral analysis, each spectrum is grouped with 25 counts per spectral channel using the `specgroup`⁵ tool of SAS.

3 RESULTS

3.1 Timing analysis

3.1.1 Variability and hardness–intensity diagram

We study the variability properties of all the sources considered in this work. First, we generate background-subtracted 200 s binned EPIC-pn light curves in 0.3–10 keV energy range. Next, to deduce the variability properties of the sources, we calculate the fractional rms variability amplitude, $F_{\text{var}} = \left(\sqrt{S^2 - \sigma_{\text{err}}^2} \right) / \bar{x}$, following Vaughan et al. (2003) and Bhuvana et al. (2021). Here, \bar{x} , S^2 , and σ_{err}^2 are the mean count rate, variance, and associated error of the light curve. We find that the sources exhibit distinct variability properties with

F_{var} varying in a wide range of 4.11–93.85 per cent including all the four sources and NGC 4395 ULX-1 remains the most variable source (see Table 1). Note that a similar study on the BH-ULX variability indicates $F_{\text{var}} \sim 1.42$ –27.28 per cent for the rest of the five sources (see Paper I). In Figs 1(a) and (b), we depict the background-subtracted 200 s binned light curves of NGC 55 ULX-1 and NGC 4395 ULX-1, respectively, for the representation of variability in BH-ULXs. It is noteworthy that for most of the sources, marginal variability is observed and hence we refrain from presenting the light curves of the remaining sources in Fig. 1.

Further, we generate the hardness–intensity diagram (HID) by defining the hardness ratio as $\text{HR} = C_1/C_2$ with C_1 and C_2 being the background-subtracted count rates in 2–10 and 0.3–2 keV energy ranges, respectively. In Fig. 1(c), the HID of the respective sources is presented using different coloured open circles. The data points in the HID of NGC 6946 X-1, NGC 1313 X-1, IC 342 X-1, and NGC 5408 X-1 are adopted from the results presented in Paper I for comparison. We observe that each source shows a distinct pattern in the HID. In particular, NGC 55 ULX-1 and NGC 5408 X-1 roughly show $\text{HR} \lesssim 0.15$, and IC 342 X-1 exhibits a relatively harder nature with $\text{HR} \sim 1$, whereas the rest of the sources remain confined within $0.15 \lesssim \text{HR} \lesssim 0.6$ in the HID. We observe that the HID of NGC 55 ULX-1 and NGC 4395 ULX-1 differ from the other sources, as they coarsely exhibit a ‘C-shaped’ pattern (see Fig. 1c). Indeed, three of the most recent observations of NGC 4395 ULX-1 show fainter characteristics at higher energies ($\gtrsim 2$ keV; see Section 4.2) and remain as outliers ($\text{HR} \sim 0.07$) from the ‘C-shaped’ pattern in the HID. Note that the intensity of these two sources varies significantly with HR, whereas the remaining sources do not show such variations. On the other hand, an apparent negative correlation is observed between HR and the count rate of NGC 5204 X-1, NGC 1313 X-1, and IC 342 X-1, respectively.

3.1.2 Power density spectra

The power spectral properties, including QPO features, are extensively studied for the five BH-ULXs, namely NGC 1313 X-1, NGC 5408 X-1, M82 X-1, NGC 6946 X-1, and IC 342 X-1 in Paper I. Following a similar approach, we investigate the power density spectrum (PDS) of the observations for the remaining four sources (NGC 55 ULX-1, NGC 5204 X-1, NGC 4395 ULX-1, and NGC 4190 ULX-1) using EPIC-pn data in 0.3–10 keV energy range. The PDS of the individual sources shows a constant Poisson noise power within 1.64–1.96 and a power-law distribution towards the low frequency, which are modelled with a constant and power-law components, respectively. However, no significant variability is seen for a few observations of the sources (see Table 1), and a constant component is found to be sufficient to fit the PDS. In Fig. 2, we depict the PDS of the sources in different colours for respective epochs. Further, we estimate the total percentage rms amplitude of the PDS in the 0.001–0.1 Hz frequency range for the individual sources and find it to vary within 22.61–50.29 per cent.

(i) *Possible detection of QPO.* Interestingly, we notice that in one of the observation (XMM2) of NGC 55 ULX-1, significant excess in power remains near ~ 0.02 Hz after fitting the continuum with a power-law and constant components for a χ^2_{red} of $167/125 = 1.34$. Hence, to fit the observed feature, we include one Lorentzian component near ~ 0.02 Hz. In general, each Lorentzian component is defined with three parameters, namely the centroid frequency (LC), width (LW), and normalization (LN). With this, the resultant fit is obtained for an improved χ^2_{red} of $156/122 = 1.28$ with the

²<https://heasarc.gsfc.nasa.gov/db-perl/W3Browse/w3browse.pl>

³<https://www.cosmos.esa.int/web/xmm-newton/sas-threads>

⁴<https://www.cosmos.esa.int/web/xmm-newton/sas>

⁵<https://xmm-tools.cosmos.esa.int/external/sas/current/doc/specgroup/index.html>

Table 1. Details of the *XMM-Newton* observations analysed in this work of the four selected BH-ULXs. In the table, all the symbols have their usual meanings. The ticks in the remarks column indicate the cleaned and good-quality data available for the analysis. Here, F_{var} is not estimated for the observations affected by high particle background flares, and the corresponding columns are filled with ‘–’ symbol. Similarly, $\text{Total}_{\text{rms}}$ is not estimated when PDS is modelled only with a constant component and for such cases, the respective column is filled using ‘–’. See the text for details.

Source	Mission	ObsID	Epoch	Date	MJD	Exposure (ks)	Rate (counts s ⁻¹) (0.3–10 keV)	F_{var}	Total _{rms} (per cent)	Remarks
NGC 55 ULX-1	<i>XMM-Newton</i>	0028740201	XMM1	2001-11-14	52227.63	30.4	1.80 ± 0.23	16.39 ± 1.84	24.11 ± 2.88	✓
		0028740101	XMM2	2001-11-15	52228.05	26.1	1.94 ± 0.33	21.09 ± 2.38	22.61 ± 0.92	✓
		0655050101	XMM3	2010-05-24	55340.32	113.7	0.91 ± 0.16	10.16 ± 6.15	50.29 ± 1.47	✓
		0824570101	XMM4	2018-11-17	58439.62	108.9	0.66 ± 0.14	5.98 ± 2.23	45.36 ± 1.73	✓
		0852610101	XMM5	2019-11-27	58814.87	4.7	1.69 ± 0.23	10.02 ± 1.32	–	✓
		0852610201	XMM6	2019-12-27	58844.52	4.8	1.72 ± 0.24	9.80 ± 1.44	–	✓
		0852610301	XMM7	2020-05-11	58980.93	5.8	0.70 ± 0.15	9.34 ± 3.94	–	✓
		0852610401	XMM8	2020-05-19	58988.40	4.8	1.66 ± 0.34	12.22 ± 3.14	–	✓
		0864810101	XMM9	2020-05-24	58993.92	117.7	0.92 ± 0.16	16.42 ± 6.29	45.79 ± 3.16	✓
		0883960101	XMM10	2021-12-12	59560.31	130	1.14 ± 0.11	5.65 ± 2.75	48.21 ± 13.77	✓
NGC 4395 ULX-1	<i>XMM-Newton</i>	0112521901	XMM1	2002-05-31	52425.03	13.9	0.27 ± 0.09	9.03 ± 3.18	–	Poor statistics
		0112522001	XMM2	2002-06-12	52437.76	17.1	–	–	–	Obs. affected by particle flares
		0112522701	XMM3	2003-01-03	52642.93	6.7	0.29 ± 0.09	11.23 ± 8.24	–	Poor statistics
		0142830101	XMM4	2003-11-30	52973.14	103.4	0.33 ± 0.11	4.11 ± 1.19	44.22 ± 5.18	✓
		07444010101	XMM5	2014-12-28	57019.42	53.5	–	–	–	Source is offset in CCD frame
		07444010201	XMM6	2014-12-30	57021.42	53	–	–	–	Source is offset in CCD frame
		0824610101	XMM7	2018-12-13	58465.26	112.8	0.40 ± 0.12	16.83 ± 6.87	25.65 ± 3.32	✓
		0824610201	XMM8	2018-12-19	58471.24	113.6	0.47 ± 0.11	81.17 ± 4.59	41.55 ± 2.13	✓
		0824610301	XMM9	2018-12-31	58483.22	110.5	0.38 ± 0.27	93.85 ± 57.71	45.18 ± 6.28	✓
		0824610401	XMM10	2019-01-02	58485.21	105.9	0.76 ± 0.16	25.67 ± 6.64	36.54 ± 5.64	✓
		0913600101	XMM11	2022-12-10	59923.34	33	0.31 ± 0.07	12.74 ± 4.36	37.78 ± 12.22	✓
		0913600501	XMM12	2022-12-14	59927.98	30	0.31 ± 0.16	10.65 ± 5.24	35.58 ± 6.53	✓
		0913600601	XMM13	2022-12-19	59932.32	38.8	0.22 ± 0.07	15.57 ± 5.38	39.04 ± 12.93	✓
		0913600701	XMM14	2022-12-22	59935.65	28	0.26 ± 0.06	7 ± 4	40.38 ± 17.66	✓
		0913600801	XMM15	2022-12-26	59939.86	28	0.24 ± 0.08	8.14 ± 1.58	32.23 ± 7.93	✓
		0913600901	XMM16	2022-12-30	59943.59	28	–	–	–	Obs. affected by particle flares
		0932391701	XMM17	2024-06-01	60462.76	43	0.26 ± 0.05	8.28 ± 4.07	39.57 ± 7.02	✓
		0932391801	XMM18	2024-06-02	60463.69	36	–	–	–	Obs. affected by particle flares
NGC 5204 X-1	<i>XMM-Newton</i>	0142770101	XMM1	2003-01-06	52645.05	16.9	0.66 ± 0.13	4.90 ± 1.38	–	✓
		0142770301	XMM2	2003-04-25	52754.57	≤ 1	–	–	–	Low exposure data
		0150650301	XMM3	2003-05-01	52760.18	2.9	1.11 ± 0.17	4.16 ± 3.13	28.41 ± 1.62	✓
		0405690101	XMM4	2006-11-15	54054.85	1.9	1.37 ± 0.19	~0.42	–	✓
		0405690201	XMM5	2006-11-19	54058.84	35.7	1.13 ± 0.18	5.11 ± 1.23	36.45 ± 7.38	✓
		0405690501	XMM6	2006-11-25	54064.82	15.9	0.83 ± 0.14	5.25 ± 1.42	46.96 ± 3.73	✓
		0693851401	XMM7	2013-04-21	56403.21	15	0.66 ± 0.13	7.64 ± 6.57	–	✓
		0693850701	XMM8	2013-04-29	56411.19	11.3	0.70 ± 0.13	5.01 ± 1.22	–	✓
		0741960101	XMM9	2014-06-27	56835.95	21.3	0.64 ± 0.13	2.04 ± 1.12	–	✓
		0921360101	XMM10	2023-05-18	60082.92	123	0.77 ± 0.15	2.74 ± 1.12	43.51 ± 7.88	✓
		0921360201	XMM11	2023-11-10	60258.43	122	0.95 ± 0.21	4.82 ± 1.78	32.44 ± 8.72	✓
NGC 4190 ULX-1	<i>XMM-Newton</i>	0654650101	XMM1	2010-06-06	55553.51	21.1	–	–	–	Obs. affected by particle flares
		0654650201	XMM2	2010-06-08	55555.47	9.8	1.05 ± 0.17	4.29 ± 1.82	–	✓
		0654650301	XMM3	2010-11-25	55525.06	5.8	1.77 ± 0.25	6.53 ± 1.12	–	✓

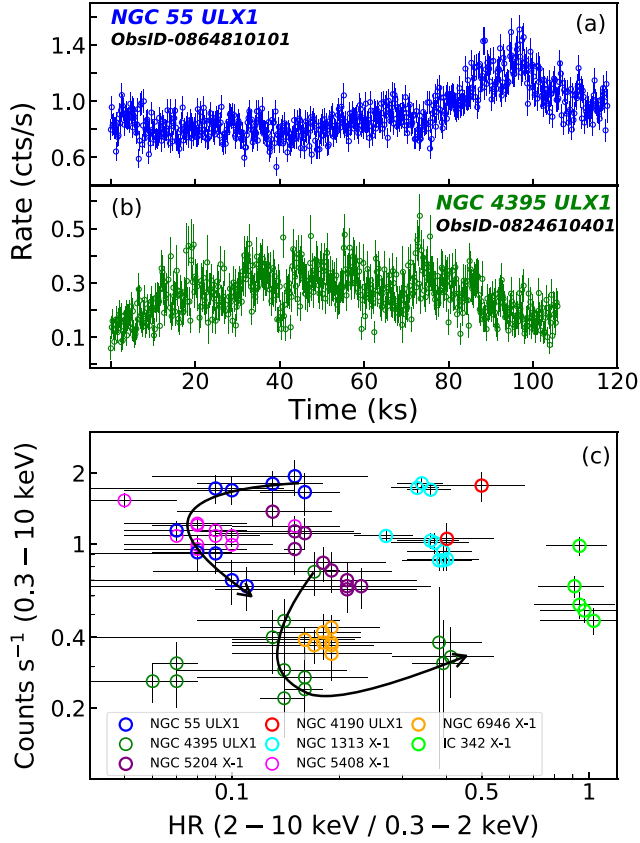


Figure 1. Panels (a) and (b): Background-subtracted 200 s binned EPIC-pn light curves of NGC 55 ULX-1 and NGC 4395 ULX-1 in 0.3–10 keV energy range. Panel (c): HID of all eight BH-ULXs considered in this work. The open circles of different colours denote the HID of the respective sources. The results for NGC 6946 X-1, NGC 1313 X-1, IC 342 X-1, and NGC 5408 X-1 are adopted from Paper I. In panel (c), the black curved arrows represent the ‘C-shaped’ patterns observed in the HID of NGC 55 ULX-1 and NGC 4395 ULX-1, respectively. See the text for details.

best-fitting Lorentzian centroid frequency of $20.43^{+1.26}_{-1.67}$ mHz. Next, we calculate the significance ($\text{LN}/\text{err}_{\text{neg}}$, where err_{neg} being the negative error in normalization), rms amplitude, and quality factor ($Q = \text{LC}/\text{LW}$) (Belloni, Sanna & Méndez 2012; Sreehari et al. 2019; Majumder et al. 2022; Paper I) of the fitted feature and obtained as 2.8σ , 6.63 per cent, and 6.68, respectively. Based on the observed high Q -factor and strength of the feature (rms percentage ~ 6.63), we interpret it as the possible detection of a QPO characteristic in NGC 55 ULX-1. For the remaining observations of the respective sources, power spectra remain featureless without any detection of QPO.

3.2 Spectral analysis

3.2.1 Spectral modelling

We model the *XMM-Newton* spectra in 0.3–10 keV energy range of all the available observations for each source using XSPEC v12.13.1 (Arnaud 1996) in HEASOFT v6.32.1. The necessary background spectra, instrument response, and ancillary files are also used while doing the spectral modelling. Both EPIC-pn and EPIC-MOS spectra are simultaneously fitted by including a `constant` component to adjust the calibration offset between the instruments. It is worth

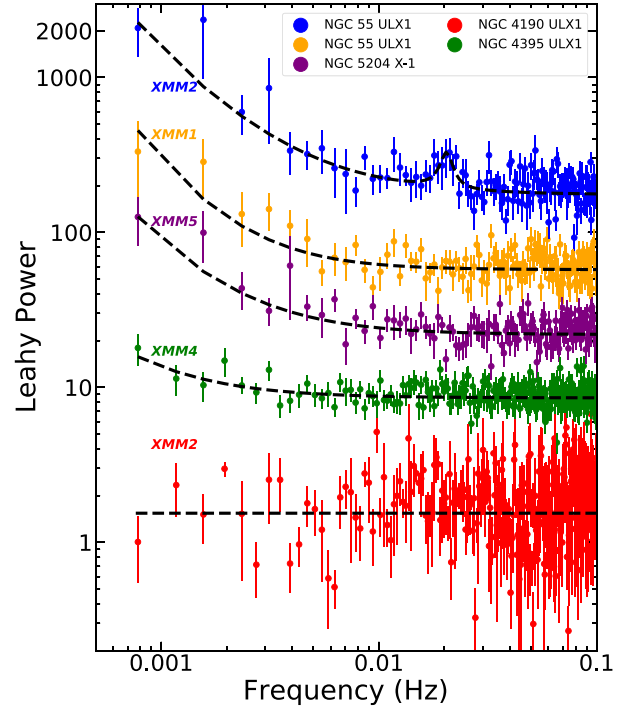


Figure 2. The PDS of NGC 55 ULX-1, NGC 5204 X-1, NGC 4395 ULX-1, and NGC 4190 ULX-1 is depicted with different colours in respective epochs. Each PDS is fitted with the combination of `constant`, `powerlaw`, and `Lorentzian` components as needed. The powers corresponding to the first four PDS presented from top to bottom are rescaled with the constant multiplicative factors of 100, 32, 12, and 4.5, respectively, for better clarity. See the text for details.

mentioning that the individual spectra of EPIC-pn, EPIC-MOS1, and EPIC-MOS2 are not combined for spectral fitting.

In the modelling, we consider the model combination, `constant × Tbbabs × (diskbb + nthComp)`, comprising of a thermal Comptonization component (`nthComp` in XSPEC; Zdziarski, Johnson & Magdziarz 1996) and a standard disc component (`diskbb` in XSPEC; Makishima et al. 1986). Here, `Tbbabs` takes care of the intergalactic absorption column and the absorption local to the source (Wilms, Allen & McCray 2000). It is worth mentioning that a similar model formalism is found to provide the best fit of the *XMM-Newton* spectra for the other four sources (NGC 5408 X-1, NGC 1313 X-1, NGC 6946 X-1, and IC 342 X-1) as presented in Paper I. Hence, we proceed to generalize the model prescription for all the BH-ULXs considered in this work. While doing so, the seed photon temperature of `nthComp` component kept tied with the inner disc temperature of the `diskbb` component during the spectral modelling. With this, the above model prescription is seen to provide the best fit for the observations of all the sources under consideration. The best-fitting model parameters and the corresponding fit statistics are tabulated in Table 2 for NGC 55 ULX-1, NGC 5204 X-1, NGC 4395 ULX-1, and NGC 4190 ULX-1. We mention that the disc contribution is observed to be negligible and the Comptonization component remains adequate to delineate the spectra in a few observations (see Table 2). In contrast, we notice that for a few observations (XMM11–XMM17) of NGC 4395 ULX-1, the disc component alone remains adequate to fit the spectra. This is mostly because of the extremely faint nature of the source in higher energies ($\gtrsim 2$ keV) during these observations, in which high-quality data remain up to $\lesssim 2$ keV only for spectral modelling. Additionally, we notice that the electron

Table 2. Best-fitting underestimated spectral parameters obtained from the simultaneous modelling of EPIC-pn and EPIC-MOS spectra of the *XMM-Newton* observations of respective sources in 0.3–10 keV energy range using the model combination $\text{constant} \times \text{TBabs} \times (\text{diskbb} + \text{nthComp})$. All the quantities mentioned in the table have their usual meanings. The flux and luminosity values are presented in units of $\times 10^{-12} \text{ erg cm}^{-2} \text{ s}^{-1}$ and $\times 10^{39} \text{ erg s}^{-1}$, respectively.

Parameters	XMM1	XMM2	XMM3	XMM4	XMM5	XMM6	XMM7	XMM8	XMM9	XMM10	XMM11
NGC 55 ULX-1											
$(D = 1.94 \text{ Mpc})$											
$n_{\text{H}} (10^{22} \text{ cm}^{-2})$	$0.16^{+0.04}_{-0.03}$	$0.33^{+0.05}_{-0.06}$	$0.11^{+0.02}_{-0.02}$	$0.15^{+0.03}_{-0.03}$	$0.38^{+0.04}_{-0.04}$	$0.41^{+0.12}_{-0.08}$	$0.43^{+0.12}_{-0.13}$	$0.40^{+0.11}_{-0.18}$	$0.11^{+0.02}_{-0.02}$	0.11^a	—
$kT_{\text{in}} (\text{keV})$	—	$0.16^{+0.02}_{-0.03}$	—	—	$0.15^{+0.03}_{-0.03}$	$0.14^{+0.03}_{-0.02}$	$0.14^{+0.01}_{-0.01}$	$0.15^{+0.03}_{-0.04}$	—	—	—
Γ_{in}	$3.01^{+0.06}_{-0.05}$	$2.65^{+0.02}_{-0.05}$	$3.64^{+0.07}_{-0.07}$	$3.42^{+0.05}_{-0.06}$	$3.27^{+0.08}_{-0.07}$	$3.31^{+0.15}_{-0.13}$	$3.32^{+0.21}_{-0.30}$	$3.31^{+0.26}_{-0.33}$	$3.56^{+0.08}_{-0.07}$	$3.48^{+0.04}_{-0.04}$	—
$kT_e (\text{keV})$	$1.62^{+0.06}_{-0.05}$	1.62^a	1.62^a	2^a	1.89^a	1.62^a	2^a	2^a	1.62^a	2^a	—
$\chi^2/\text{degrees of freedom}$	338/283	383/261	470/319	422/312	207/169	164/145	152/107	99/96	456/337	476/287	—
F_{disc}	—	2.88 ± 0.19	—	—	5.36 ± 0.49	9.03 ± 0.41	4.95 ± 0.34	7.40 ± 0.34	—	—	—
F_{in}	6.21 ± 0.14	8.39 ± 0.18	2.89 ± 0.07	2.60 ± 0.06	9.32 ± 0.21	10.04 ± 0.52	3.63 ± 0.17	5.10 ± 0.23	2.88 ± 0.19	4.71 ± 0.04	—
F_{bol}	7.46 ± 0.17	16.04 ± 0.36	3.57 ± 0.08	3.39 ± 0.08	23.62 ± 0.54	33.78 ± 0.75	16.21 ± 0.72	21.76 ± 1.47	3.58 ± 0.08	4.75 ± 0.03	—
L_{bol}	3.36 ± 0.08	7.22 ± 0.16	1.60 ± 0.04	1.53 ± 0.04	10.64 ± 0.24	15.21 ± 0.33	7.30 ± 0.32	9.81 ± 0.66	1.61 ± 0.06	2.14 ± 0.01	—
L_{disc}	—	2.44 ± 0.09	—	—	4.58 ± 0.22	8.10 ± 0.18	4.89 ± 0.16	6.51 ± 0.15	—	—	—
τ	8.32 ± 0.21	9.72 ± 0.23	6.62 ± 0.15	6.30 ± 0.13	6.88 ± 0.21	7.42 ± 0.41	6.53 ± 0.72	6.55 ± 0.79	6.80 ± 0.18	6.16 ± 0.08	—
$y\text{-par}$	0.88 ± 0.04	1.19 ± 0.06	0.55 ± 0.03	0.62 ± 0.03	0.70 ± 0.04	0.69 ± 0.08	0.67 ± 0.15	0.67 ± 0.16	0.58 ± 0.03	0.59 ± 0.02	—
NGC 5204 X-1											
$(D = 4.8 \text{ Mpc})$											
$n_{\text{H}} (10^{22} \text{ cm}^{-2})$	$0.04^{+0.02}_{-0.02}$	—	$0.05^{+0.03}_{-0.02}$	$0.06^{+0.01}_{-0.02}$	$0.06^{+0.01}_{-0.01}$	$0.04^{+0.01}_{-0.01}$	$0.06^{+0.03}_{-0.03}$	$0.04^{+0.01}_{-0.01}$	$0.04^{+0.02}_{-0.02}$	$0.06^{+0.01}_{-0.01}$	$0.07^{+0.01}_{-0.01}$
$kT_{\text{in}} (\text{keV})$	$0.26^{+0.04}_{-0.02}$	—	$0.28^{+0.06}_{-0.06}$	$0.29^{+0.05}_{-0.05}$	$0.28^{+0.05}_{-0.03}$	$0.28^{+0.05}_{-0.03}$	$0.24^{+0.04}_{-0.04}$	$0.25^{+0.05}_{-0.04}$	$0.25^{+0.04}_{-0.03}$	$0.24^{+0.01}_{-0.01}$	$0.25^{+0.03}_{-0.02}$
Γ_{in}	$1.66^{+0.13}_{-0.06}$	—	$2.07^{+0.14}_{-0.16}$	$2.16^{+0.29}_{-0.11}$	$2.12^{+0.15}_{-0.16}$	$1.85^{+0.11}_{-0.12}$	$1.69^{+0.11}_{-0.09}$	$1.77^{+0.13}_{-0.16}$	$1.76^{+0.09}_{-0.11}$	$1.79^{+0.05}_{-0.05}$	$2.17^{+0.12}_{-0.12}$
$kT_e (\text{keV})$	$1.62^{+0.38}_{-0.27}$	—	2.5^a	1.62^a	$2.07^{+1.04}_{-0.42}$	2.65^a	$1.73^{+0.49}_{-0.25}$	2.13^a	$1.98^{+0.61}_{-0.34}$	$2.09^{+0.29}_{-0.21}$	$2.49^{+0.88}_{-0.43}$
$\chi^2/\text{degrees of freedom}$	236/225	—	167/164	103/133	327/328	319/296	223/212	238/208	268/247	525/395	393/332
F_{disc}	0.46 ± 0.02	—	0.68 ± 0.05	0.95 ± 0.02	0.76 ± 0.02	0.57 ± 0.01	0.52 ± 0.02	0.42 ± 0.02	0.37 ± 0.02	0.85 ± 0.02	0.86 ± 0.03
F_{in}	1.29 ± 0.03	—	1.95 ± 0.09	2.27 ± 0.10	2.10 ± 0.05	1.58 ± 0.04	1.35 ± 0.06	1.46 ± 0.07	1.34 ± 0.03	1.76 ± 0.02	2.41 ± 0.02
F_{bol}	2.04 ± 0.03	—	3.15 ± 0.07	3.76 ± 0.09	3.37 ± 0.03	2.64 ± 0.06	2.21 ± 0.05	2.24 ± 0.05	2.02 ± 0.05	2.61 ± 0.03	3.24 ± 0.04
L_{bol}	5.62 ± 0.08	—	8.69 ± 0.02	10.37 ± 0.03	9.29 ± 0.08	7.31 ± 0.02	6.09 ± 0.14	6.18 ± 0.14	5.57 ± 0.16	7.19 ± 0.05	8.93 ± 0.03
L_{disc}	1.71 ± 0.06	—	2.48 ± 0.14	3.45 ± 0.06	2.78 ± 0.06	2.10 ± 0.03	1.98 ± 0.06	1.59 ± 0.06	1.71 ± 0.05	2.34 ± 0.04	2.37 ± 0.05
τ	18.37 ± 3.26	—	10.47 ± 1.11	12.60 ± 1.54	11.27 ± 2.42	11.89 ± 1.14	17.23 ± 3.17	14.33 ± 1.72	15.04 ± 2.35	14.24 ± 1.27	3.31 ± 0.28
$y\text{-par}$	4.27 ± 1.07	—	2.14 ± 0.46	2.01 ± 0.48	2.05 ± 0.42	2.93 ± 0.56	4.01 ± 0.83	3.42 ± 0.82	3.51 ± 0.67	3.31 ± 0.28	1.89 ± 0.28
NGC 4395											
ULX-1											
$(D = 4.76 \text{ Mpc})$											
$n_{\text{H}} (10^{22} \text{ cm}^{-2})$	—	$0.10^{+0.03}_{-0.03}$	$0.10^{+0.02}_{-0.02}$	$0.10^{+0.02}_{-0.02}$	$0.11^{+0.03}_{-0.03}$	$0.11^{+0.03}_{-0.02}$	$0.03^{+0.01}_{-0.02}$	0.03^a	0.03^a	0.05^a	0.05^a
$kT_{\text{in}} (\text{keV})$	—	$0.15^{+0.02}_{-0.02}$	$0.15^{+0.02}_{-0.02}$	$0.16^{+0.02}_{-0.02}$	$0.15^{+0.03}_{-0.03}$	—	$0.32^{+0.02}_{-0.02}$	$0.31^{+0.01}_{-0.01}$	$0.31^{+0.01}_{-0.01}$	$0.29^{+0.01}_{-0.01}$	$0.31^{+0.01}_{-0.01}$
Γ_{in}	—	$3.34^{+0.17}_{-0.18}$	$3.33^{+0.18}_{-0.16}$	$3.20^{+0.09}_{-0.08}$	$3.86^{+0.25}_{-0.29}$	$3.05^{+0.05}_{-0.05}$	—	—	—	—	—
$kT_e (\text{keV})$	—	2^a	1.92^a	2^a	2^a	1.62^a	—	—	—	—	—
$\chi^2/\text{degrees of freedom}$	—	179/155	180/155	259/212	179/146	313/237	118/77	96/86	141/87	127/79	131/108
F_{disc}	—	0.23 ± 0.02	0.24 ± 0.02	0.24 ± 0.03	0.27 ± 0.03	—	0.55 ± 0.01	0.43 ± 0.01	0.52 ± 0.01	0.49 ± 0.01	0.55 ± 0.02
F_{in}	—	0.63 ± 0.03	0.62 ± 0.02	1.34 ± 0.03	0.74 ± 0.03	1.81 ± 0.03	—	—	—	—	—
F_{bol}	—	1.37 ± 0.03	1.40 ± 0.03	2.37 ± 0.03	1.76 ± 0.04	2.71 ± 0.04	0.57 ± 0.01	0.45 ± 0.01	0.42 ± 0.02	0.54 ± 0.01	0.57 ± 0.02
L_{bol}	—	3.71 ± 0.08	3.80 ± 0.08	6.43 ± 0.08	4.77 ± 0.11	7.35 ± 0.08	1.55 ± 0.02	1.22 ± 0.01	1.14 ± 0.02	1.46 ± 0.02	1.38 ± 0.01
L_{disc}	—	1.27 ± 0.05	1.31 ± 0.03	1.28 ± 0.04	1.61 ± 0.05	—	1.49 ± 0.02	1.17 ± 0.01	1.11 ± 0.02	1.41 ± 0.02	1.33 ± 0.01
τ	—	6.48 ± 0.41	6.67 ± 0.44	6.83 ± 0.23	5.43 ± 0.51	8.13 ± 0.16	—	—	—	—	—
$y\text{-par}$	—	0.66 ± 0.08	0.67 ± 0.09	0.73 ± 0.05	0.46 ± 0.08	0.85 ± 0.03	—	—	—	—	—

Table 2 – continued

Parameters	XMM2	XMM3	XMM4	XMM7	XMM8	XMM9	XMM10	XMM11	XMM12	XMM13	XMM14	XMM15	XMM17
n_{H} (10^{22} cm $^{-2}$)						NGC 4190 ULX-1 ($D = 3$ Mpc)							
Γ_{nth}	$0.06^{+0.01}_{-0.01}$	$0.15^{+0.06}_{-0.02}$											
kT_{e} (keV)	$2.09^{+0.19}_{-0.12}$	$1.69^{+0.03}_{-0.03}$											
kT_{c} (keV)	1.62^a	$1.67^{+0.11}_{-0.11}$											
$\chi^2/\text{degrees of freedom}$	317/293	335/337											
F_{nth}	3.31 ± 0.06	7.13 ± 0.09											
F_{bol}	3.53 ± 0.07	8.17 ± 0.12											
L_{bol}	3.80 ± 0.07	8.79 ± 0.13											
τ	13.16 ± 1.61	17.56 ± 0.79											
$y\text{-par}$	2.19 ± 0.53	4.03 ± 0.23											

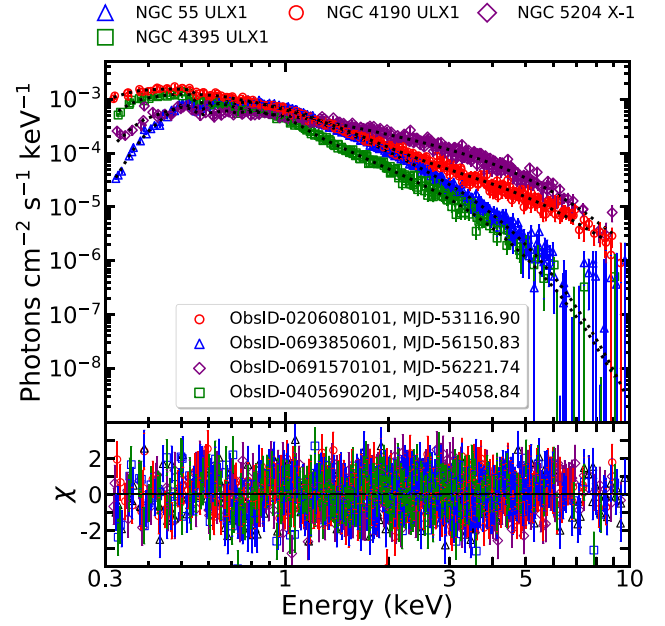
^aFrozen to best-fitting value.

Figure 3. Top: Best-fitting EPIC-pn and EPIC-MOS energy spectra of the four sources plotted simultaneously in 0.3–10 keV energy range. Each spectrum is modelled using the model combination $\text{constant} \times \text{Tbabs} \times (\text{diskbb} + \text{nthComp})$. Bottom: Variation of residuals (in units of σ) obtained from the best fit of the individual spectra. See the text for details.

temperature remains unconstrained in most of the observations and, hence, frozen to the best-fitting values. Notably, in a few observations (XMM1, XMM3, XMM4, and XMM9) of NGC 55 ULX-1, an absorption edge is required to adjust the residuals near ~ 1 keV (Jithesh 2022). In contrast, a Gaussian line is used to fit the broad emission feature observed at ~ 1 keV in all the spectra of NGC 4395 ULX-1 (Ghosh et al. 2022). The best-fitting energy spectra of NGC 55 ULX-1, NGC 4395 ULX-1, NGC 5204 X-1, and NGC 4190 ULX-1 are shown in Fig. 3 for the purpose of representation. Further, we compute the flux associated with different model components, optical depth, and Compton y -parameter following Paper I. Also, the total and disc bolometric luminosities are estimated from the flux values, assuming the well-constrained source distances (see Table 2).

3.2.2 Spectral properties

In general, spectral features of the sources are well described by standard accretion disc and thermal Comptonization components, very similar to the spectral morphologies of a group of BH-ULXs presented in Paper I. We find that the spectral modelling results the photon index (Γ_{nth}) in the range of $1.66^{+0.13}_{-0.06}$ – $3.86^{+0.25}_{-0.29}$ and the inner disc temperature (kT_{in}) varies within $0.14^{+0.01}_{-0.01}$ – $0.32^{+0.02}_{-0.02}$ keV for NGC 55 ULX-1, NGC 4395 ULX-1, NGC 5204 X-1, and NGC 4190 ULX-1 (see Table 2). Note that similar model formalism, used to fit the spectra of the remaining sources (NGC 1313 X-1, NGC 5408 X-1, NGC 6946 X-1, and IC 342 X-1), results in the electron temperature (kT_{e}), Γ_{nth} , and kT_{in} in the range of 1.62–3.76 keV, 1.48–2.65, and 0.16–0.54 keV, respectively (see Paper I for details). Further, the optical depth and Compton y -parameter are found to be within $6 \lesssim \tau \lesssim 20$ and $0.46 \lesssim y\text{-par} \lesssim 6.24$ considering all the sources (see Table 2 and Paper I). This suggests that the presence of a relatively cool accretion disc and optically thick corona are the generic features

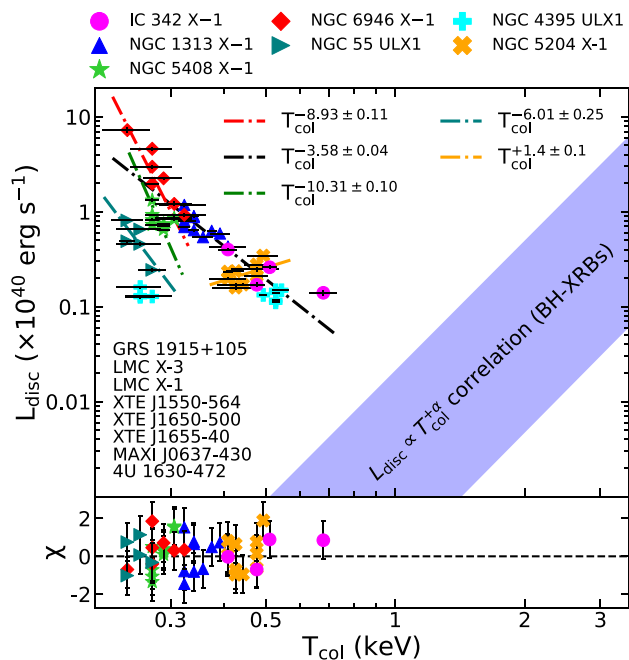


Figure 4. Correlation between the bolometric disc luminosity and colour-corrected inner disc temperature of all BH-ULXs. The dash-dot lines of different colours represent the best fit in describing the $L_{\text{disc}}-T_{\text{col}}$ distribution of each source with the functional form mentioned in the figure. The blue-shaded region represents the correlation between the luminosity and disc temperature of the form $L_{\text{disc}} \propto T_{\text{col}}^{+\alpha}$ for eight BH-XRBs, adopted from Gierliński & Done (2004), Abe et al. (2005), Vierdayanti, Mineshige & Ueda (2010), and Baby et al. (2021). See the text for details.

of the BH-ULXs considered for this work (Gladstone, Roberts & Done 2009).

3.2.3 Spectral correlation

In this section, we attempt to deduce intrinsic correlations among the best-fitting and estimated spectral parameters for the respective sources. In doing so, we use the results obtained from the spectral analysis (see Section 3.2.1) of NGC 55 ULX-1, NGC 5204 X-1, and NGC 4395 ULX-1, presented in Table 2 along with the findings reported from the detailed spectral modelling of four BH-ULXs (NGC 1313 X-1, NGC 5408 X-1, NGC 6946 X-1, and IC 342 X-1) in Paper I (see table 4). We investigate the correlation between the bolometric disc luminosity (L_{disc}) and colour-corrected disc temperature (T_{col}) of the respective sources. Note that the inner disc temperature (T_{in}) is multiplied with the spectral hardening factor ($f_c = 1.7$) following Done & Davis (2008) and Davis & El-Abd (2019) to obtain the T_{col} . In Fig. 4, we present the obtained results, where the L_{disc} (in $\times 10^{40} \text{ erg s}^{-1}$) is plotted as a function of T_{col} (in keV).

We notice the trend of possible correlations of distinct characteristics between L_{disc} and T_{col} for all the sources. To deduce the firmness of the correlations, we estimate the Pearson correlation coefficient (ρ) of the distributions in $L_{\text{disc}}-T_{\text{col}}$ plane for the respective cases (see Paper I). It is found that the source NGC 55 ULX-1 shows a negative correlation between L_{disc} and T_{col} with $\rho \sim -0.74$. However, the variation in L_{disc} is found to be marginal for NGC 4395 ULX-1 and the corresponding distribution in the $L_{\text{disc}}-T_{\text{col}}$ plane appears to form two distinct regimes of lower and higher temperatures (see

Fig. 4), indicating no evidence of correlation with $\rho \sim -0.11$ only. It may be noted that the higher disc temperatures ($\sim 0.3 \text{ keV}$) are obtained for the observations in which only the disc component fits the entire spectra of narrow energy coverage ($\sim 0.3-2 \text{ keV}$) in NGC 4395 ULX-1. Therefore, the two distinct regions of different disc temperatures (see Fig. 4) perhaps resulted from the difference in model prescriptions for the respective cases. Contrarily, NGC 5204 X-1 is seen to exhibit a clear positive correlation with $\rho \sim +0.7$. Moreover, a strong negative correlation is obtained with $\rho \sim -0.81$ for the combined results of NGC 1313 X-1 and IC 342 X-1, and $\rho \sim -0.89$ for NGC 6946 X-1. Although we find a weak anticorrelation with $\rho \sim -0.27$ in $L_{\text{disc}}-T_{\text{col}}$ plane of NGC 5408 X-1.

Further, we proceed to delineate the observed correlations of the sources with the empirical power-law profile $L_{\text{disc}} \propto T_{\text{col}}^{\alpha}$ (Rybicki & Lightman 1979) using the `curve_fit`⁶ module in PYTHON. The individual fits result the power-law exponent (α) as -6.01 ± 0.25 , -8.93 ± 0.11 , -10.31 ± 0.10 , and 1.4 ± 0.1 for NGC 55 ULX-1, NGC 6946 X-1, NGC 5408 X-1, and NGC 5204 X-1, respectively. However, the combined fitting of the correlation distributions for IC 342 X-1 and NGC 1313 X-1 indicates $\alpha = -3.58 \pm 0.04$. It may be noted that because of the marginal variation observed in L_{disc} and T_{col} , we refrain from modelling the luminosity–temperature distribution for NGC 4395 ULX-1. In Fig. 4, we present the best-fitting power-law functional form in the top panel for the respective sources and the residuals in the bottom panel, respectively. In addition, we show the positive correlation between the disc luminosity and temperature of the form $L_{\text{disc}} \propto T_{\text{col}}^{+\alpha}$, typically observed for BH-XRBs, with a blue shade in Fig. 4. Note that the data associated with these correlation properties are adopted from Gierliński & Done (2004), Abe et al. (2005), Vierdayanti et al. (2010), and Baby et al. (2021) and the disc temperature values are colour-corrected using the same hardening factor ($f_c = 1.7$), considered for this work.

3.2.4 Evolution of spectral properties

We study the long-term spectral evolution of the eight BH-ULXs, namely NGC 1313 X-1, IC 342 X-1, NGC 4395 ULX-1, NGC 5408 X-1, NGC 55 ULX-1, NGC 4190 ULX-1, NGC 6946 X-1, and NGC 5204 X-1 using the *XMM-Newton* observations over a decade. In Fig. 5, the variation of inner disc temperature (kT_{in} in keV), electron temperature (kT_e in keV), photon index (Γ_{nth}), disc flux (F_{disc} in $\text{erg cm}^{-2} \text{ s}^{-1}$), Comptonized flux (F_{nth} in $\text{erg cm}^{-2} \text{ s}^{-1}$), Compton y -parameter (y -par), and bolometric luminosity (L_{bol} in erg s^{-1}) are depicted from top to bottom panels, respectively, over different epochs of observation. We mention that the best-fitting spectral parameters of NGC 1313 X-1, IC 342 X-1, NGC 5408 X-1, and NGC 6946 X-1 are adopted from the results presented in Paper I (see table 4 of that paper). However, for the rest of the sources, the best-fitting parameters are tabulated in Table 2.

We observe that the spectral properties of the BH-ULXs generally exhibit significant variation over the long-term evolution of the sources and manifest several spectral states. In particular, we find the dominance of the Comptonization flux over the disc contribution ($F_{\text{nth}} \gtrsim F_{\text{disc}}$) for NGC 5204 X-1, IC 342 X-1, NGC 4190 ULX-1, and NGC 1313 X-1, respectively. As expected, the photon index is observed to be in the harder limit of $\Gamma_{\text{nth}} \lesssim 2$, and the y -par, indicative of the amount of Comptonization, remains $\gtrsim 2$

⁶https://docs.scipy.org/doc/scipy/reference/generated/scipy.optimize.curve_fit.html

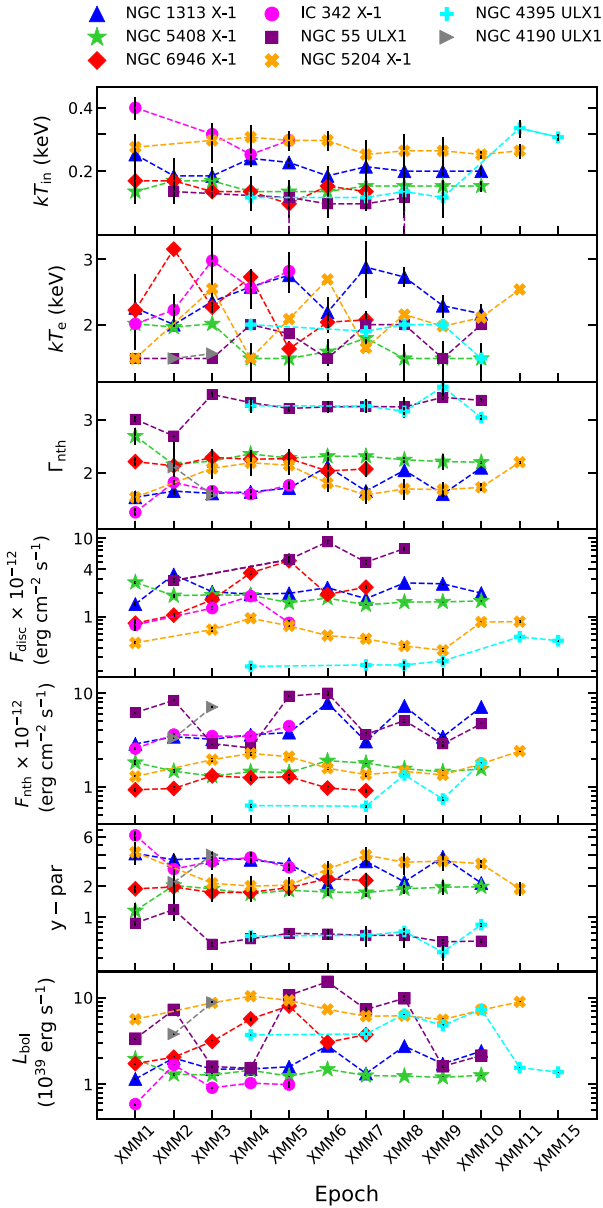


Figure 5. Evolution of the spectral parameters over the long-term monitoring is shown with distinct coloured markers for the respective sources. The variation of inner disc temperature, electron temperature, photon index, disc flux, Comptonized flux, Compton y -parameter, and bolometric luminosity over different epochs is shown from top to bottom panels, respectively. See the text for details.

for all the four sources (see Fig. 5). Further, we find a low disc temperature ($kT_{\text{in}} \lesssim 0.3$ keV) for these sources, except NGC 4190 ULX-1, in which the disc is absent and Comptonization contribution is noticeably high. In contrast, NGC 6946 X-1 manifests disc-dominated spectral characteristics with $F_{\text{disc}} \gtrsim F_{\text{nth}}$ and $\Gamma_{\text{nth}} \gtrsim 2$ (see Fig. 5). Interestingly, comparable disc and Comptonized flux contributions are seen in the spectra of NGC 55 ULX-1 and NGC 5408 X-1. However, the source NGC 55 ULX-1 replicates relatively softer nature with $\Gamma_{\text{nth}} \gtrsim 3$ and $y\text{-par} \lesssim 1$, whereas NGC 5408 X-1 remains in the intermediate regime ($F_{\text{disc}} \approx F_{\text{nth}}$, $\Gamma_{\text{nth}} \lesssim 2$, and $1 < y\text{-par} \lesssim 2$). Finally, for NGC 4395 ULX-1, we observe a negligible disc contribution with $y\text{-par} \lesssim 1$ and high photon index

($\Gamma_{\text{nth}} \gtrsim 3$). This possibly resulted from the appearance of broad emission feature at lower energy (~ 1 keV), suggesting distinct and rather complex spectral characteristics of NGC 4395 ULX-1. Note that the spectral parameters of NGC 4395 ULX-1 show marginal variations during later epochs (XMM11–XMM17; see Fig. 2), hence we present only the results for XMM11 and XMM15 in Fig. 5. A significant variation in the luminosity is noticed over the entire observation period of more than a decade for most of the sources. Note that a low electron temperature within $1 \lesssim kT_e \lesssim 3$ keV is obtained for all the sources, indicating the presence of a relatively cool Compton corona, generally seen in ULXs.

4 DISCUSSION

In this work, we study the long-term evolution of the spectrottemporal properties of eight BH-ULXs using *XMM-Newton* observations spanning over a decade or more. The detailed spectral analyses reveal the presence of significant correlations between the colour-corrected inner disc temperature (T_{col}) and the associated disc luminosity (L_{disc}) of the sources. The long-term spectral evolution study infers that different spectral states seem to be connected with the observed correlation properties of the respective sources.

We investigate the variability properties of four BH-ULXs, namely NGC 55 ULX-1, NGC 4395 ULX-1, NGC 5204 X-1, and NGC 4190 ULX-1 in detail. For these sources, the fractional variability amplitude is found to vary as 4.11–93.85 per cent. A similar study for the remaining sources (i.e. NGC 1313 X-1, NGC 5408 X-1, NGC 6946 X-1, and IC 342 X-1) were already carried out in Paper I, where the fractional variability is obtained as 1.42–27.28 per cent. The HID presented in Fig. 1(c) indicates an apparent anticorrelation between the count rate and HR for NGC 5408 X-1, NGC 1313 X-1, NGC 5204 X-1, and IC 342 X-1, respectively. Further, the power spectral study reveals the total percentage rms variability amplitude as 22–50 per cent in 0.001–0.1 Hz frequency range for all BH-ULXs under consideration.

Furthermore, a detailed PDS investigation reveals the detection of a moderately significant ($\sigma \sim 2.8$, rms percentage ~ 6.63) QPO-like feature at ~ 20 mHz in NGC 55 ULX-1 during Epoch XMM2. Interestingly, for this source, the PDS resembles the characteristics of a QPO (see Section 3.1), although such a feature is not observed within a day during its previous observation. It is worth mentioning that NGC 1313 X-1, NGC 5408 X-1, NGC 6946 X-1, M82 X-1, and IC 342 X-1 manifest prominent QPO features of frequency ~ 8 –667 mHz over different observation epochs of *XMM-Newton* (Atapin et al. 2019; Paper I, and references therein).

4.1 Long-term evolution of BH-ULXs

The long-term evolution of spectral properties and the flux contributions from different spectral components confirm the presence of soft, intermediate, and hard spectral states in the BH-ULXs. In particular, we observe that NGC 5204 X-1, IC 342 X-1, NGC 4190 ULX-1, and NGC 1313 X-1 remain within the group of ULXs, showing harder spectral features with dominant effects of thermal Comptonization ($y\text{-par} \gtrsim 2$) and relatively weak disc emission ($F_{\text{disc}} \lesssim F_{\text{nth}}$; see Table 2 and Fig. 5). Moreover, the flatter photon index ($\Gamma_{\text{nth}} \lesssim 2$) possibly indicates the presence of a Comptonizing tail similar to BH-XRBs spectra in their hard/intermediate states (Remillard & McClintock 2006). With this, we infer that for these BH-ULXs, an optically thick Comptonizing corona residing at the inner region of a low-temperature ($0.2 \lesssim kT_{\text{in}} \lesssim 0.4$) disc appears to be the preferred accretion scenario with harder spectral characteristics.

In contrast, we find disc-dominated spectral morphologies in NGC 6946 X-1, where the disc flux is roughly twice the Comptonized flux and $\Gamma_{\text{nth}} \gtrsim 2$. Indeed, such classification of the sources based on the spectral flux contribution is similar to the SUL and HUL states (Sutton et al. 2013). Notably, NGC 6946 X-1 is observed in the disc-dominated state in the absence of a high-energy spectral break in most of the previous studies, and has been identified as a persistent ULX with softer characteristics (Earnshaw et al. 2019; Ghosh & Rana 2023). Finally, the intermediate spectral nature ($F_{\text{disc}} \approx F_{\text{nth}}$, $\Gamma_{\text{nth}} \lesssim 2$, and $1 < y\text{-par} \lesssim 2$) is observed for NGC 5408 X-1 over the long-term monitoring, which is identified as the intermediate-ultraluminous (IUL) state, whereas NGC 55 ULX-1 remains in the SUL state. We note that the presence of a ‘bright hard intermediate state’ is reported for NGC 5408 X-1 (Caballero-García, Belloni & Zampieri 2013) and NGC 55 ULX-1 is found to manifest a steep photon index ($\Gamma > 3$) in the previous studies (Jithesh 2022), which are consistent with the present findings.

4.2 Correlation between L_{disc} and T_{col} in BH-ULXs

The variation of L_{disc} with T_{col} affirms the distinct correlation for all the BH-ULXs under consideration. In particular, all the sources, except NGC 5204 X-1, show a negative correlation in the $L_{\text{disc}}-T_{\text{col}}$ plane, while a clear positive correlation is observed for NGC 5204 X-1. The best-fitting correlations with the empirical power-law distribution $L_{\text{disc}} \propto T_{\text{col}}^{\alpha}$ yield the exponent as $\alpha = -8.93$ (NGC 6946 X-1), $\alpha = -6.01$ (NGC 55 ULX-1), $\alpha = -10.31$ (NGC 5408 X-1), $\alpha = +1.4$ (NGC 5204 X-1), and $\alpha = -3.58$ (combined IC 342 X-1 and NGC 1313 X-1), respectively (see Fig. 4). It is noteworthy that NGC 4395 ULX-1 manifests marginal variation in the disc luminosity and temperature over different observations with $\rho \sim -0.11$ only, and hence we discard it from the present discussion.

We further note that a negative correlation between L_{disc} and T_{col} yielding a power-law exponent of -3.5 is reported for several ULXs (Kajava & Poutanen 2009) that remains consistent with this study. Interestingly, we observe an apparent connection between the correlation properties, and the spectral states of the individual sources. For example, steeper ($\alpha < -4$) anticorrelations are seen for the sources in SUL (NGC 6946 X-1 and NGC 55 ULX-1) and IUL (NGC 5408 X-1) spectral states, respectively. However, a more flat power-law exponent ($\alpha \sim -4$) is noticed for IC 342 X-1 and NGC 1313 X-1 in the HUL state. In addition, NGC 5204 X-1 manifests a positive correlation in the HUL state.

Meanwhile, several galactic BH-XRBs, such as XTE J1550–564, XTE J1650–500, GRO J1655–40, GX 339–4, XTE J1859+226 Gierliński & Done (2004), and MAXI J0637–430 (Baby et al. 2021), show clear positive correlations between L_{disc} and T_{col} . This is also true for extragalactic sources like LMC X-1 and LMC X-3 (Gierliński & Done 2004). These correlations align with the predictions of standard disc theory (Shakura & Sunyaev 2009). Interestingly, depending on the luminosity, 4U 1630–472 (Abe et al. 2005), XTE J1550–564 (Kubota & Makishima 2004), and GRS 1915+105 (Vierdayanti et al. 2010) are observed to follow or deviate from the standard $L_{\text{disc}} \propto T_{\text{col}}^4$ correlation in different observations. In particular, when the luminosity is close to the Eddington limit, the sources are observed to exhibit a flatter correlation of the form $L_{\text{disc}} \propto T_{\text{col}}^2$ (Watarai, Mizuno & Mineshige 2001).

4.3 Possible dichotomy in $L_{\text{disc}} \propto T_{\text{col}}^{\alpha}$ correlation

In this study, we observe both positive and negative correlations between L_{disc} and T_{col} for all BH-ULXs under consideration. Needless

to mention that the appearance of ‘unusual’ correlation, including anticorrelations ($-\alpha$), leads to the possible dichotomy between the present findings and the existing theoretical frameworks. The BH-XRBs are also seen to deviate from the standard picture on several occasions, as pointed out in the preceding section. Never the less, several attempts have been made to explain this, although the origin of the dichotomy remains elusive. Depending on α , the correlations are coarsely summarized in three different regimes for several BH-XRBs and BH-ULXs and briefly described as

$$\begin{aligned} \alpha &= 4 && \text{(standard disc),} \\ L_{\text{disc}} \propto T_{\text{col}}^{\alpha}; \quad 0 \leq \alpha < 4 && \text{(slim disc),} \\ -10 \leq \alpha < 0 && \text{(anomalous).} \end{aligned}$$

(i) *Standard disc scenario.* Needless to mention that the luminosity associated with the disc emission is expected to follow $L_{\text{disc}} \propto T_{\text{col}}^4$ as predicted from the standard accretion disc prescription (Shakura & Sunyaev 2009). In general, the Keplerian disc component of the accretion flow locally emits as a multicolour blackbody at different disc radii, resulting in the expected correlation (Frank, King & Raine 2002).

(ii) *Slim disc scenario.* Several BH-XRBs, including 4U 1630–472, XTE J1550–564, and GRS 1915+105, are seen to deviate from the standard disc and mostly follow a flatter correlation as $2 \lesssim \alpha < 4$ (Kubota & Makishima 2004; Abe et al. 2005; Vierdayanti et al. 2010). It has also been suggested that different accretion scenarios exist for these BH-XRBs, which determine the nature of the correlations. In this study, we observe that NGC 5204 X-1 is the only BH-ULX that manifests a positive correlation of the form $L_{\text{disc}} \propto T_{\text{col}}^{1.4}$, however, this relation is not generally determined by the spectral states. Moreover, at relatively higher luminosity, close to the Eddington limit, the deviation from $\alpha \sim 4$ becomes more prominent (Kubota & Makishima 2004). A geometrically thin ($H/r \ll 1$) and radiatively efficient standard Keplerian disc is characterized by a moderately low accretion rate. However, the ‘slim disc’ appears with relatively higher luminosity ($\gtrsim 0.3L_{\text{Edd}}$), yielding thicker disc geometry ($H/r \lesssim 1$), where the angular momentum remains sub-Keplerian (Abramowicz et al. 1988; Chakrabarti 1995; Beloborodov 1998; Abramowicz & Fragile 2013). Interestingly, a more flat correlation, i.e. $L_{\text{disc}} \propto T_{\text{col}}^2$, is predicted for such discs (Watarai et al. 2001). Therefore, a possible explanation of the observed anomaly in the deviation of the power-law exponent could be the transition from the standard disc ($\alpha \sim 4$) to the ‘slim disc’ scenario ($\alpha \sim 2$).

(iii) *Anomalous scenario.* Intriguingly, the negative correlations with $\alpha < 0$ observed in several BH-ULXs offer challenges, with only a few attempts made to explain these findings. King & Puchnarewicz (2002) proposed that the anticorrelation ($\alpha \sim -4$) may possibly result in due to the strong beamed emission in ULXs. Interestingly, the detection of coherent QPO features in BH-ULXs (Atapin et al. 2019; Paper I) indicates the presence of an axisymmetric geometrically thin accretion disc, which contradicts the presence of strong beaming (Matteo & Psaltis 1999; Strohmayer & Mushotzky 2003). Furthermore, Middleton et al. (2019) reported that the Lense–Thirring precession of the inner accretion flow can be attributed to the origin of the QPOs in ULXs. Meanwhile, Das et al. (2021) argued that the aperiodic modulation of the inner hot ‘Comptonizing corona’ successfully explains QPO features of BH-ULXs. All these findings clearly indicate the need for an alternative model of accretion dynamics to explain the negative α values in the presence of QPO features.

Table 3. Summary of the observed correlation properties between L_{disc} and T_{col} in different spectral states and the predicted inclinations of the BH-ULXs.

Source	Spectral state ^a	$L_{\text{disc}}-T_{\text{col}}$ correlation exponent (α)	Predicted inclination
NGC 5204 X-1	HUL	1.4 ± 0.1	Low
IC 342 X-1	HUL	-3.58 ± 0.04	Moderate
NGC 1313 X-1	HUL	-3.58 ± 0.04	Moderate
NGC 55 ULX-1	IUL	-6.01 ± 0.25	High
NGC 6946 X-1	SUL	-8.93 ± 0.11	High
NGC 5408 X-1	IUL	-10.31 ± 0.10	High
NGC 4190 ULX-1	HUL	–	Low
M82 X-1	–	–	Low
NGC 4395 ULX-1	HUL	–	Moderate

^aHUL: hard-ultraluminous state; SUL: soft-ultraluminous state; IUL: intermediate-ultraluminous state. See Sutton et al. (2013).

4.4 Alternative physical scenario

The limitations of the standard disc and slim disc models in explaining $L_{\text{disc}}-T_{\text{col}}$ correlations prompt us to explore alternative physically motivated accretion–ejection model prescriptions for BH-ULXs. Such a model prescription appears to be capable of explaining the overall spectrotimporal properties, including $L_{\text{disc}}-T_{\text{col}}$ correlation and QPO features.

The accretion–ejection model formalism relies on the coexistence of Keplerian and sub-Keplerian flows (Chakrabarti & Titarchuk 1995) and it explains the aspects of spectrotimporal variabilities of BH-XRBs (Chakrabarti & Manickam 2000; Chakrabarti, Dutta & Pal 2009; Debnath, Chakrabarti & Nandi 2010; Nandi et al. 2012; Iyer, Nandi & Mandal 2015; Sreehari et al. 2019, and references therein). Similarly, this model is expected to explain the spectrotimporal variabilities of BH-ULXs. Further, the non-steady modulation of the Comptonizing corona (with radius r_s), formed by the sub-Keplerian component, leads to aperiodic variations in the emitted hard X-rays, which may give rise to QPO features (Molteni, Sponholz & Chakrabarti 1996; Lee, Ryu & Chattopadhyay 2011; Das et al. 2014; Garain, Ghosh & Chakrabarti 2014; Debnath, Chattopadhyay & Joshi 2024). This conjecture effectively explains the mHz QPOs, which have become key observables for constraining the mass, spin, and accretion rate in several BH-ULXs (Das et al. 2021; Paper I). Moreover, by regulating the Keplerian and sub-Keplerian flow components and depending on system inclinations, different spectral states (HUL, SUL, and IUL) can be identified for BH-ULXs (see Table 3). Furthermore, powerful winds are also expected to eject from (a) the boundary of hot coronal region in the inner accretion flow (Chakrabarti 1999; Das et al. 2001, 2014; Chattopadhyay & Chakrabarti 2002), (b) standard thin Keplerian disc (Proga, Stone & Drew 1998; Yang, Bu & Li 2018; Raychaudhuri, Vyas & Chattopadhyay 2021), and (c) super-Eddington (supercritical) slim disc (Poutanen et al. 2007; Dotan & Shaviv 2011), respectively. Moreover, we mention that a model formalism in the framework of relativistic dissipative accretion flow around a rotating black hole has been developed to interpret the luminosity and mHz QPO characteristics of BH-ULXs (Das et al. 2021; Paper I). However, a more comprehensive modelling of the spectral energy distribution to explain the observed spectral characteristics of BH-ULXs is yet to be developed. We depict a schematic representation of the accretion–ejection configuration for the BH-ULXs in Fig. 6.

For supercritical accretion state of BH-ULXs, the slim disc model seems relevant, where radiation pressure balances gravity at the spherization radius (r_{sp}) resulting in a sub-Keplerian geometrically thick ($H/r \lesssim 1$) disc at $r_s \leq r \leq r_{\text{sp}}$ (see Fig. 6 and Fabrika et al.

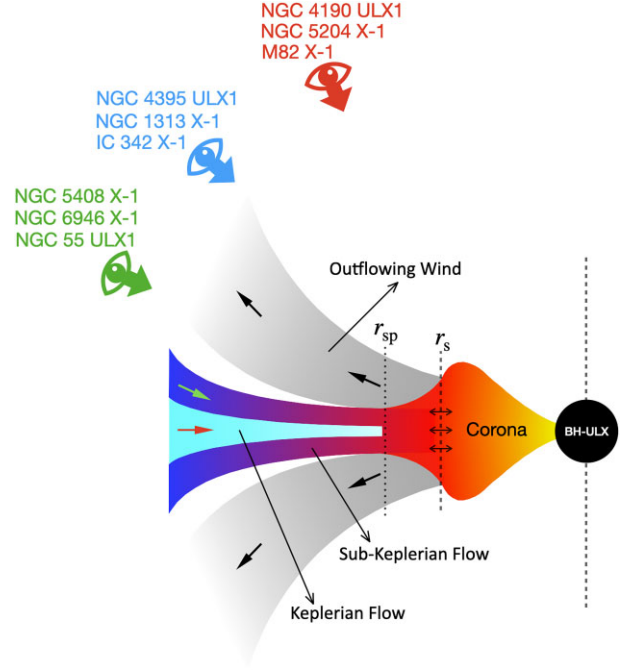


Figure 6. Schematic representation of disc–corona–wind-regulated two-component accretion scenario of BH-ULXs. Thick arrows in green, blue, and red colours represent the viewing angles of the observer corresponding to high, moderate, and low inclinations of sources, respectively. The red, green, and black small arrows indicate the direction of the Keplerian flow, sub-Keplerian flow, and winds. Here, r_s and r_{sp} denote the boundary of the corona and spherization radius. The region $r_{\text{sp}} < r < r_s$ refers the geometrically thick ‘slim disc’. The two-sided black arrows show the radial oscillation of the coronal region around r_s . See the text for details.

2021). With this, it is apparent that the emission associated with the Keplerian disc ($r > r_{\text{sp}}$) is consistent with the standard disc prediction ($L_{\text{disc}} \propto T_{\text{col}}^4$), whereas the interplay between the inner slim disc and the standard disc at larger radii likely leads to the deviation observed as $L_{\text{disc}} \propto T_{\text{col}}^{1.4}$ for NGC 5204 X-1. As NGC 4190 ULX-1 and NGC 5204 X-1 are observed in the HUL state throughout their long-term spectral evolution (see Section 4.1), the inner Comptonizing corona, which is the source of non-thermal emission, at $r < r_s$ is expected to be visible to the observer, suggesting a low inclination for these two sources (see Fig. 6). In addition, the absence of QPO features in NGC 4190 ULX-1 and NGC 5204 X-1 possibly indicates that the radial modulation of the coronal region is either absent or very feeble to be detected. A similar accretion scenario seems to be relevant for M82 X-1 with the exception that oscillation of the corona is prominent enough to produce the observed mHz QPOs (Paper I). Indeed, the prediction of M82 X-1 inclination from the spectral analysis using *XMM-Newton* data could be uncertain because of high contamination. However, it may be noted that M82 X-1 exhibits coherent mHz QPO features on several occasions that are perhaps associated with the Comptonizing corona (see Paper I). Further, the *Chandra* resolved spectra of the source prefer a slim disc scenario over the standard accretion disc (Brightman et al. 2016). These evidences possibly suggest that M82 X-1 could be a low inclination system, where the inner Comptonizing corona coupled with a slim accretion disc is visible to the observer, somewhat similar to the case of NGC 5204 X-1.

In the presence of winds, the emitted radiations from the disc interact substantially with the outflowing matter before reaching the

observer. Due to this, the thermal emission is expected to be cooler with increasing luminosity for supercritical discs in the presence of strong outflowing winds (Poutanen et al. 2007). Considering this, the bolometric luminosity (L_{bol}) is estimated as

$$L_{\text{bol}} \approx L_{\text{Edd}} \left(1 + \frac{3}{5} \ln \dot{m}_0 \right); \quad T_{\text{col}} \approx 1.5 f_c m^{-1/4} \dot{m}_0^{-1/2}, \quad (1)$$

where T_{col} denote the colour-corrected temperature at the spherization radius, and $\dot{m}_0 (= \dot{M}_0 / \dot{M}_{\text{Edd}} \gg 1)$ is the accretion rate. Here, f_c , L_{Edd} , and m are the spectral hardening factor, Eddington luminosity, and mass of the central object scaled in solar mass, respectively. Note that equation (1) leads to an anticorrelation between L_{bol} and T_{col} , with a steeper exponent (α) (Poutanen et al. 2007). Furthermore, the outflows from the region $r < r_{\text{sp}}$ appear to remain optically thick, and a part of the energy generated within the disc is carried away by the winds. This process is expected to reduce the disc temperature and modify the disc luminosity.

The relatively flatter negative correlations ($\alpha \sim -3.58$) observed in the HUL state of IC 342 X-1, NGC 1313 X-1, and NGC 4395 ULX-1 suggest an accretion–ejection scenario, where the primary emission is significantly influenced by disc winds. However, the existence of the HUL state indicates that a part of the coronal emission is directly accessible to the observer, suggesting a moderate inclination of the sources (see Fig. 6 and Table 3). In contrast, for NGC 55 ULX-1, NGC 5408 X-1, and NGC 6946 X-1, the steeper negative correlations ($-10 \lesssim \alpha \lesssim -6$) in the SUL/IUL state likely indicate significant modification of the primary emission due to enhanced winds covering the line of sight. This suggests relatively higher inclinations for these sources (see Fig. 6 and Table 3). In both scenarios, it is plausible that the outflowing winds could carry the imprints of oscillations in the Comptonizing region, as predicted by Das et al. (2014), thereby providing a self-consistent explanation for the QPO features observed in IC 342 X-1, NGC 1313 X-1, NGC 5408 X-1, and NGC 6946 X-1. However, the irregular appearance of QPOs throughout the entire *XMM–Newton* monitoring of these sources (see Paper I) suggests that either the necessary resonance condition for modulating the coronal region is not being satisfied, or the oscillation is weak enough to remain undetected.

Moreover, we speculate that the disc–corona–wind symbiosis for the two-component supercritical accretion scenario seems to be realistic to explain the spectrottemporal features of BH-ULXs across different spectral states. We also indicate that radiative pressure-driven winds from the supercritical disc possibly govern the correlation between disc luminosity and temperature, and such correlation depends on the source inclination. This conjecture further strengthens the possibility of having a super-Eddington accretion scenario with massive stellar-mass to intermediate-mass black hole accretors in NGC 5408 X-1, NGC 6946 X-1, IC 342 X-1, and NGC 1313 X-1, as predicted in Paper I.

5 CONCLUSION

In this study, we carry out a comprehensive analysis of the long-term evolution of eight BH-ULXs using *XMM–Newton* observations. Our findings provide compelling evidence for varied accretion scenarios that can explain the observed spectrottemporal variability and (anti)correlations between disc luminosity (L_{disc}) and inner disc temperature (T_{col}). The key results from our investigation, along with their potential implications, are summarized below.

(i) The positive correlation of $L_{\text{disc}} \propto T_{\text{col}}^{1.4}$ observed for NGC 5204 X-1 suggests a transition from the standard geometrically thin disk

($H/r \ll 1$) to a slim disk ($H/r \lesssim 1$) prescription at relatively higher luminosities in the HUL state. This behaviour is reminiscent of an accretion scenario where both Keplerian and sub-Keplerian flow components coexist.

(ii) A steeper negative correlation with $-10 \lesssim \alpha \lesssim -6$ between L_{disc} and T_{col} is observed for sources NGC 6946 X-1, NGC 55 ULX-1, and NGC 5408 X-1, which exhibit softer and intermediate spectral characteristics. In contrast, a relatively flatter anticorrelation with $\alpha \sim -3.58$ is seen for IC 342 X-1 and NGC 1313 X-1, which display harder spectral features.

(iii) The diverse $L_{\text{disc}}-T_{\text{col}}$ correlations along with the overall spectrottemporal characteristics suggest a connection with the disc–corona–wind-regulated two-component supercritical accretion scenario. Such a scenario is also potentially viable to explain the observed QPO features in BH-ULXs. In particular, we infer that the anticorrelations are possibly a result of the modification of disc emissions by the outflowing winds, which is also likely to be influenced by moderate to high inclinations of the respective BH-ULXs.

ACKNOWLEDGEMENTS

The authors thank the anonymous reviewer for constructive comments and useful suggestions that helped to improve the quality of the paper. SM and SD thank the Department of Physics, IIT Guwahati, for providing the facilities to complete this work. AN thanks GH, SAG, DD, PDMSA, and Director URSC for encouragement and continuous support to carry out this research. This publication uses the data from the *XMM–Newton* mission, archived at the HEASARC data center. The instrument team is thanked for processing and providing useful data and software for this analysis.

DATA AVAILABILITY

Data used for this publication are currently available at the HEASARC browse website (<https://heasarc.gsfc.nasa.gov/db-perl/W3Browse/w3browse.pl>).

REFERENCES

- Abe Y., Fukazawa Y., Kubota A., Kasama D., Makishima K., 2005, *PASJ*, 57, 629
- Abramowicz M. A., Fragile P. C., 2013, *Living Rev. Relativ.*, 16, 1
- Abramowicz M. A., Czerny B., Lasota J. P., Szuszkiewicz E., 1988, *ApJ*, 332, 646
- Agrawal V. K., Nandi A., 2015, *MNRAS*, 446, 3926
- Alston W. N. et al., 2021, *MNRAS*, 505, 3722
- Aneasha U., Das S., Katoch T. B., Nandi A., 2024, *MNRAS*, 532, 4486
- Arnaud K. A., 1996, in Jacoby G. H., Barnes J., eds, *ASP Conf. Ser. Vol. 101*, Astronomical Data Analysis Software and Systems V. Astron. Soc. Pac., San Francisco, p. 17
- Atapin K., Fabrika S., Caballero-García M. D., 2019, *MNRAS*, 486, 2766
- Athulya M. P., Radhika D., Agrawal V. K., Ravishankar B. T., Naik S., Mandal S., Nandi A., 2022, *MNRAS*, 510, 3019
- Baby B. E., Bhuvana G. R., Radhika D., Katoch T., Mandal S., Nandi A., 2021, *MNRAS*, 508, 2447
- Bachetti M. et al., 2013, *ApJ*, 778, 163
- Bachetti M. et al., 2014, *Nature*, 514, 202
- Barra F. et al., 2022, *MNRAS*, 516, 3972
- Belloni T., Homan J., Casella P., van der Klis M., Nespoli E., Lewin W. H. G., Miller J. M., Méndez M., 2005, *A&A*, 440, 207
- Belloni T. M., Sanna A., Méndez M., 2012, *MNRAS*, 426, 1701
- Beloborodov A. M., 1998, *MNRAS*, 297, 739

- Bhuvana G. R., Radhika D., Agrawal V. K., Mandal S., Nandi A., 2021, *MNRAS*, 501, 5457
- Brightman M. et al., 2016, *ApJ*, 829, 28
- Caballero-García M. D., Belloni T., Zampieri L., 2013, *MNRAS*, 436, 3262
- Carpano S., Haberl F., Maitra C., Vasilopoulos G., 2018, *MNRAS*, 476, L45
- Chakrabarti S. K., 1995, preprint ([arXiv:astro-ph/9502040](https://arxiv.org/abs/astro-ph/9502040))
- Chakrabarti S. K., 1999, *A&A*, 351, 185
- Chakrabarti S. K., Manickam S. G., 2000, *ApJ*, 531, L41
- Chakrabarti S., Titarchuk L. G., 1995, *ApJ*, 455, 623
- Chakrabarti S. K., Dutta B. G., Pal P. S., 2009, *MNRAS*, 394, 1463
- Chattopadhyay I., Chakrabarti S. K., 2002, *J. Astrophys. Astron.*, 23, 149
- Colbert E. J. M., Mushotzky R. F., 1999, *ApJ*, 519, 89
- Das S., Chattopadhyay I., Nandi A., Chakrabarti S. K., 2001, *A&A*, 379, 683
- Das S., Chattopadhyay I., Nandi A., Molteni D., 2014, *MNRAS*, 442, 251
- Das S., Nandi A., Agrawal V. K., Dihingia I. K., Majumder S., 2021, *MNRAS*, 507, 2777
- Davis S. W., El-Abd S., 2019, *ApJ*, 874, 23
- Debnath D., Chakrabarti S. K., Nandi A., 2010, *A&A*, 520, A98
- Debnath S., Chattopadhyay I., Joshi R. K., 2024, *MNRAS*, 528, 3964
- Dewangan G. C., Titarchuk L., Griffiths R. E., 2006, *ApJ*, 637, L21
- Done C., Davis S. W., 2008, *ApJ*, 683, 389
- Dotan C., Shaviv N. J., 2011, *MNRAS*, 413, 1623
- Earnshaw H. M., Roberts T. P., 2017, *MNRAS*, 467, 2690
- Earnshaw H. P. et al., 2019, *ApJ*, 881, 38
- Earnshaw H. P. et al., 2024, *ApJ*, 968, 111
- Fabbiano G., 1989, *ARA&A*, 27, 87
- Fabrika S. N., Atapin K. E., Vinokurov A. S., Sholukhova O. N., 2021, *Astrophys. Bull.*, 76, 6
- Feng H., Kaaret P., 2009, *ApJ*, 696, 1712
- Feng H., Soria R., 2011, *New Astron. Rev.*, 55, 166
- Feng H., Rao F., Kaaret P., 2010, *ApJ*, 710, L137
- Frank J., King A., Raine D. J., 2002, *Accretion Power in Astrophysics*, 3rd edn. Cambridge Univ. Press, Cambridge
- Fürst F. et al., 2016, *ApJ*, 831, L14
- Garain S. K., Ghosh H., Chakrabarti S. K., 2014, *MNRAS*, 437, 1329
- Ghosh T., Rana V., 2021, *MNRAS*, 504, 974
- Ghosh T., Rana V., 2023, *ApJ*, 949, 78
- Ghosh T., Rana V., Bachetti M., 2022, *ApJ*, 938, 76
- Gierliński M., Done C., 2004, *MNRAS*, 347, 885
- Gladstone J. C., Roberts T. P., Done C., 2009, *MNRAS*, 397, 1836
- Grisé F., Kaaret P., Corbel S., Cseh D., Feng H., 2013, *MNRAS*, 433, 1023
- Gürpide A., Godet O., Koliopanos F., Webb N., Olive J. F., 2021, *A&A*, 649, A104
- Heil L. M., Vaughan S., Roberts T. P., 2009, *MNRAS*, 397, 1061
- Israel G. L. et al., 2017, *Science*, 355, 817
- Iyer N., Nandi A., Mandal S., 2015, *ApJ*, 807, 108
- Jithesh V., 2022, *MNRAS*, 509, 5166
- Kaaret P., Feng H., 2009, *ApJ*, 702, 1679
- Kaaret P., Feng H., Roberts T. P., 2017, *ARA&A*, 55, 303
- Kajava J. J. E., Poutanen J., 2009, *MNRAS*, 398, 1450
- King A. R., Puchnarewicz E. M., 2002, *MNRAS*, 336, 445
- King A., Lasota J.-P., Middleton M., 2023, *New Astron. Rev.*, 96, 101672
- Kosec P., Pinto C., Fabian A. C., Walton D. J., 2018, *MNRAS*, 473, 5680
- Kubota A., Makishima K., 2004, *ApJ*, 601, 428
- Lee S.-J., Ryu D., Chattopadhyay I., 2011, *ApJ*, 728, 142
- Majumder S., Sreehari H., Aftab N., Katoch T., Das S., Nandi A., 2022, *MNRAS*, 512, 2508
- Majumder S., Das S., Agrawal V. K., Nandi A., 2023, *MNRAS*, 526, 2086 (Paper I)
- Makishima K., Maejima Y., Mitsuda K., Bradt H. V., Remillard R. A., Tuohy I. R., Hoshi R., Nakagawa M., 1986, *ApJ*, 308, 635
- Makishima K. et al., 2000, *ApJ*, 535, 632
- Matteo T. D., Psaltis D., 1999, *ApJ*, 526, L101
- Middleton M. J., Heil L., Pintore F., Walton D. J., Roberts T. P., 2015, *MNRAS*, 447, 3243
- Middleton M. J., Fragile P. C., Ingram A., Roberts T. P., 2019, *MNRAS*, 489, 282
- Miller J. M., Fabbiano G., Miller M. C., Fabian A. C., 2003, *ApJ*, 585, L37
- Molteni D., Sponholz H., Chakrabarti S. K., 1996, *ApJ*, 457, 805
- Mukherjee E. S. et al., 2015, *ApJ*, 808, 64
- Nandi A., Debnath D., Mandal S., Chakrabarti S. K., 2012, *A&A*, 542, A56
- Pasham D. R., Cenko S. B., Zoghbi A., Mushotzky R. F., Miller J., Tombesi F., 2015, *ApJ*, 811, L11
- Poutanen J., Lipunova G., Fabrika S., Butkevich A. G., Abolmasov P., 2007, *MNRAS*, 377, 1187
- Proga D., Stone J. M., Drew J. E., 1998, *MNRAS*, 295, 595
- Quintin E., Webb N. A., Gürpide A., Bachetti M., Fürst F., 2021, *MNRAS*, 503, 5485
- Rana V. et al., 2015, *ApJ*, 799, 121
- Rao F., Feng H., Kaaret P., 2010, *ApJ*, 722, 620
- Raychaudhuri S., Vyas M. K., Chattopadhyay I., 2021, *MNRAS*, 501, 4850
- Remillard R. A., McClintock J. E., 2006, *ARA&A*, 44, 49
- Rodríguez Castillo G. A. et al., 2020, *ApJ*, 895, 60
- Rybicki G. B., Lightman A. P., 1979, *Radiative Processes in Astrophysics*. Wiley, New York
- Sathyaprakash R. et al., 2019, *MNRAS*, 488, L35
- Shakura N. I., Sunyaev R. A., 2009, *A&A*, 500, 33 (special issue 500/01: reprint of 1973, *A&A*, 24, 337)
- Soria R., Ghosh K. K., 2009, *ApJ*, 696, 287
- Sreehari H., Ravishankar B. T., Iyer N., Agrawal V. K., Katoch T. B., Mandal S., Nandi A., 2019, *MNRAS*, 487, 928
- Strohmayer T. E., Mushotzky R. F., 2003, *ApJ*, 586, L61
- Strohmayer T. E., Mushotzky R. F., Winter L., Soria R., Uttley P., Cropper M., 2007, *ApJ*, 660, 580
- Sutton A. D., Roberts T. P., Middleton M. J., 2013, *MNRAS*, 435, 1758
- Vaughan S., Edelson R., Warwick R. S., Uttley P., 2003, *MNRAS*, 345, 1271
- Vierdayanti K., Mineshige S., Ueda Y., 2010, *PASJ*, 62, 239
- Walton D. J. et al., 2013, *ApJ*, 779, 148
- Walton D. J. et al., 2014, *ApJ*, 793, 21
- Walton D. J. et al., 2015, *ApJ*, 799, 122
- Watarai K.-y., Mizuno T., Mineshige S., 2001, *ApJ*, 549, L77
- Wilms J., Allen A., McCray R., 2000, *ApJ*, 542, 914
- Winter L. M., Mushotzky R. F., Reynolds C. S., 2006, *ApJ*, 649, 730
- Xu Y. et al., 2019, *ApJ*, 879, 93
- Yang X.-H., Bu D.-F., Li Q.-X., 2018, *ApJ*, 867, 100
- Yoshida T., Ebisawa K., Matsushita K., Tsujimoto M., Kawaguchi T., 2010, *ApJ*, 722, 760
- Zdziarski A. A., Johnson W. N., Magdziarz P., 1996, *MNRAS*, 283, 193

This paper has been typeset from a \LaTeX file prepared by the author.